RSC Advances

PAPER

View Article Online
View Journal | View Issue

Check for updates

Cite this: *RSC Adv.*, 2017, **7**, 44605

Bentonite-supported nanoscale zero-valent iron granulated electrodes for industrial wastewater remediation

Zexu Chi,[a] Zhen Wang,[*ab] Huanqing Chu,[a] Pingping Bin[a] and Lucia Lucian[c]

Bentonite-supported nanoscale zero-valent iron (B-nZVI) granulated electrodes were synthesized for remediation of pulp and paper wastewater as part of a three-dimensional (3D) electrode system. Results of scanning electron microscopy (SEM) and energy dispersive spectrometry (EDS) suggested that the layered structure of bentonite can reduce the aggregation of nZVI effectively. X-ray diffraction (XRD) results indicated that bentonite can effectively prevent the nZVI from being oxidized. The potential of zero charge (PZC) and cation exchange capacity (CEC) suggested that B-nZVI has good adsorption performance and reactivity to remediate the pollutants in pulp and paper wastewater. The 3D electrode system exhibited high efficiency in reducing COD and color to meet emission standards. The optimum conditions were as follows: current density = 40 mA cm^{-2}, electrolysis time = 50 min, distance of electrode plates = 4 cm, granulated electrode dosage = 2 g L^{-1} and initial pH = 3.0. The maximum removal efficiencies of COD and color were 85.1% and 97.5%, respectively.

Received 10th July 2017
Accepted 11th September 2017

DOI: 10.1039/c7ra07584g

rsc.li/rsc-advances

Open Access Article. Published on 15 September 2017. Downloaded on 4/2/2026 6:58:39 AM.
This article is licensed under a Creative Commons Attribution 3.0 Unported Licence.

1. Introduction

Pulp and paper wastewater often contains high levels of toxic pollutants such as resin acids, tannins or what is produced during the manufacturing processes (*e.g.*, chlorinated organic compounds).[1] Commonly, pulp and paper wastewater requires secondary treatment consisting of physical treatment and biochemical treatment. However, the main indicators (COD, color, *etc.*) are still high even after the secondary treatment. Pollutants such as AOX, PAHs, and chromogenic lignin and its derivatives are still hard to degrade. Thus, extended treatment of the secondary effluent is critical.

Compared with traditional methods, the electrochemical method has become a hot focus due to its simplicity and ease of operation, high efficiency and eco-friendly characteristics.[2–4] It provides a high efficiency for removing bio-refractory organic pollutants.[5] Compared to conventional electrode methods, granulated electrodes in a 3D system have much shorter inter-electrode distances to allow faster electron transfer rates leading to faster remediation.[6] Previous studies showed that 3D electrodes were successfully applied to treat various industrial wastewater such as petroleum refinery wastes, dye wastes, phenolic resin wastes, phenol wastes, and heavy metal-containing solutions.[7–10] Although the materials of the granulated electrodes are quite different, they all have common characteristics such as high specific surface area, good chemical stability, and high conductivity.[11,12]

Nanoscale zero-valent iron (nZVI), because of its high surface energy, high conductivity and large specific surface area, possesses a great potential to act as granulated electrodes.[13,14] Unfortunately, nZVI granules are inclined to aggregate and oxidate, thus decreased their performance in application. Therefore, various immobilization strategies have been developed to solve this problem, such as chitosan-stabilized nZVI,[15] montmorillonite-supported nZVI,[16] and carboxymethyl cellulose (CMC) stabilized nZVI.[17] Bentonite is one of the abundant and low-cost clay minerals that possesses high adsorption, conductivity and stability.[18,19] It has a unique layered structure which is suitable for the loading, fixation and padding of nZVI. In our previous research, we described the application of cetyl trimethyl ammonium bromide modified bentonite in a 3D system as granulated electrodes for the treatment of pulp and paper wastewater and achieved satisfactory results.[19]

The purpose of this study was to synthesize bentonite-supported nanoscale zero-valent iron (B-nZVI) and apply it to a 3D electrode system as granulated electrodes to remediate pulp and paper wastewater. The whole process was divided into two parts: determination of optimum conditions in two-dimensional (2D) electrode system (part 1), followed by addition of B-nZVI into the 2D electrode system to form a 3D system for treatment of pulp and paper wastewater (part 2). The main impact factors including current density, electrolysis time,

[a]*Key Laboratory of Pulp & Paper Science and Technology, Qilu University of Technology, Jinan, Shandong Province 250353, P. R. China. E-mail: wangzhenyft@126.com; Tel: +86 15864791007*

[b]*Key Laboratory of Cleaner Production and Industrial Waste Recycling and Resourcing, University of Shandong (Qilu University of Technology), China*

[c]*Department of Forest Biomaterials, North Carolina State University, Box 8005, Raleigh, NC 27695-8005, USA*

Open Access Article. Published on 15 September 2017. Downloaded on 4/2/2026 6:58:39 AM. This article is licensed under a Creative Commons Attribution 3.0 Unported Licence.

distance of electrode plates, dosage of B-nZVI, and initial pH of wastewater on removal efficiency of COD and color were explored. To further verify the efficacy of 3D system, the wastewater before and after treatment was analyzed by gas chromatograph-mass spectrometry (GC-MS). Finally, a possible mechanism for the treatment of pulp and paper wastewater using 3D system with B-nZVI granulated electrodes was posited.

2. Materials and methods

2.1 Reagents

Sodium bentonite (Na-bentonie) was purchased from Guangfu chemical research institute (Tianjin, China). The cation exchange capacity (CEC) was 87.4 mmol/100 g. The chemical composition was qualified. Dichloromethane was chromatographic grade and other reagents were analytical grade, including iron(III) chloride hexahydrate ($FeCl_3 \cdot 6H_2O$), sodium borohydride ($NaBH_4$), and ethyl alcohol.

Wastewater was from a pulp and paper mill secondary sedimentation tank, Yatai Senbo Co. Ltd, Shandong, China. Table 1 showed the main characteristics of the wastewater before and after treatment.

2.2 Synthesis

B-nZVI was synthesized using liquid-phase reduction method with bentonite as a support material.[20] First, to obtain B-nZVI (iron/bentonite mass ratio of 1 : 1), 4.84 g ferric chloride hexahydrate ($FeCl_3 \cdot 6H_2O$) was dissolved in 50 mL mixture of absolute ethanol and distilled water (volume ratio was 4 : 1) and then 1.0 g of bentonite was added into it. The suspension was stirred for 10 min with the speed of 300 rpm, then 0.47 M $NaBH_4$ solution (100 mL) was added drop-wise (1–2 drops per s) into this mixture with vigorous stirring (500 rpm). Subsequently the mixture was stirred for another 20 min continuously. All of the processes should be carried out under N_2 atmosphere protection. The jet-black products were collected by vacuum filtration and needed to be rinsed three times quickly with absolute ethanol to prevent immediate oxidation of Fe^0. The prepared samples were dried at 65 °C under vacuum overnight and were kept in a nitrogen atmosphere prior to use.[21]

As a comparison, nZVI was prepared using the same method without the addition of bentonite.

2.3 Optimization of the operational parameters

The difference between 2D system and 3D system was the addition of granulated electrodes (as can be seen in Fig. 1). In addition, the electrolysis of pulp and paper wastewater was conducted in an electrolytic reaction tank of 100 × 50 × 60 mm dimensions. Ruthenium/iridium coated titanium plates (50 × 1 × 65 mm) with good electrochemical stability were used as anode and cathode electrode plates and parallel to each other.

The optimization process mainly consisted of two parts: determination of optimum conditions for 2D electrode system (part 1) and 3D electrode system (part 2) for treatment of pulp and paper wastewater. During part 1, current density, electrolysis time and distance of electrode plates were selected as factors. They were adjusted between 10–50 mA cm^{-2}, 10–60 min, 3–6 cm, respectively. Subsequently, in part 2, under the optimum conditions obtained from 2D system, B-nZVI was added to form a 3D system (Fig. 1). The effects of B-nZVI dosage and initial pH of wastewater on removal efficiency of COD and color were also explored.

The volume of wastewater fed into the electrode reactor was 100 mL for each run. After each group experiments, the treated wastewater was filtered by 0.4 μm membrane for the following detection of COD and color removal efficiencies. Following each run, the electrode plates should be washed with 0.1 M HCl and pure water, then dried and used again.

2.4 Characterization of the feed and secondary sludge

XRD patterns of Na-bentonite, fresh B-nZVI and recovered B-nZVI (after ten runs) were measured by X-ray diffraction (D8-Advance, Bruker AXS Co. Ltd, German) at 40 kV and 40 mA in step scan mode. The diffraction angle: 10° to 80° at 5°(2θ)/min. SEM and EDS analyses were applied by the Scanning Microscope apparatus (Quanta 200, FEI, USA) in order to disclose the surface morphology of bentonite, nZVI and B-nZVI. The specific surface areas of bentonite, nZVI, B-nZVI and recovered B-nZVI (after ten runs) were detected by BET-N_2 adsorption method using BET surface area and a porosimetry analyzer (V-Sorb 2800P, Beijing, China). Conductivity of bentonite was measured by a 4-point probes resistivity measurement system (RTS-8, Guangzhou, China). The potential of zero charge (PZC) of bentonite, nZVI, fresh B-nZVI and recovered B-nZVI (after ten runs) was determined using a zeta charge detector (MuetekAnalgtielnc). The cation exchange capacity (CEC) of bentonite, fresh B-nZVI and recovered B-nZVI (after ten runs) was determined by ammonium acetate exchange method.

2.5 Characterization of water quality

The species and content of organic contaminants in the wastewater were detected by gas chromatograph-mass spectrometry (GC-MS-QP2010, SHIMADZU, Japan).

First, three samples of initial wastewater (the volume of each sample was 50 mL) were prepared, the pH value of one sample

Table 1 Characteristics of pulp and paper wastewater before and after treatment

Characteristics	Color	Conductivity (μS cm^{-1})	COD (mg L^{-1})	TOC (mg L^{-1})	TDS (g L^{-1})	UV_{254} (cm^{-1})	Lignin (g L^{-1})
Before treatment	Brown	4200	296	116.9	3.52	2.587	0.07
After treatment	Clear	4400	44	15.44	0.15	0.192	0.003

 This journal is © The Royal Society of Chemistry 2017

Open Access Article. Published on 15 September 2017. Downloaded on 4/2/2026 6:58:39 AM.
This article is licensed under a Creative Commons Attribution 3.0 Unported Licence.

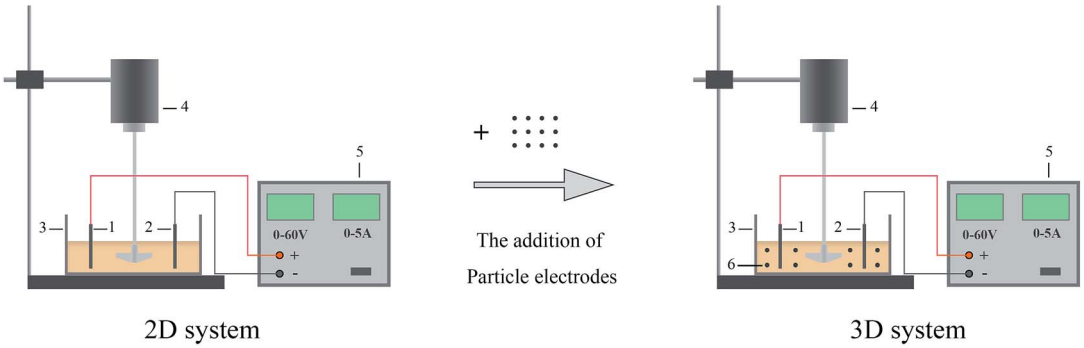

Fig. 1 Experimental apparatus of 2D system and 3D system.

was adjusted to approach 2.0 with H_2SO_4 (the ratio with deionized water was 1 : 1) and another was adjusted to approach 12.0 with NaOH (10%). After standing for 20 minutes, three samples were filtered using 0.4 μm membrane. Next, dichloromethane (50 mL) and NaCl (0.2 g) were added into all samples to extract. It was necessary to shock the mixture (4 min) and stand for stratification (6 min). The extraction process was repeated twice, then three organic phases were collected and merged together. The merged organic phase was concentrated by rotary evaporation until its volume was less than 5 mL, then 0.2 g anhydrous Na_2SO_4 was added to dehydrate for 1 h. Finally, the organic phase was filtered using 0.22 μm membrane for GC-MS detection. Similarly, the wastewater treated under optimum electrolytic conditions was also extracted using the same process.

The chromatographic column was DB-5. The chromatographic test conditions were high purity helium and CV mode at 0.086 MPa; the temperature of the injection port was 250 °C, the sample size was 1 μL and the split ratio was 30 : 1; the heating procedure was initial temperature of 40 °C and heated up to 180 °C at a temperature ramp of 10 °C per min, then heated up to 280 °C at a temperature ramp of 5 °C per min and held for 5 min. The mass spectrometer conditions were 1.2 kV electron bombardment voltage, 70 eV EI source electron bombardment energy, 30–550 amu mass scan range, and 3 min solvent delay.

Furthermore, pH was measured using a PHS-3C digital pH meter. COD was obtained through oxidation with $K_2Cr_2O_7$ under acidic conditions and titration analysis with $(NH_4)_2$-$Fe(SO_4)_2$ aqueous solution according to the national criterion of PR China (GB11914-89). And color was obtained by the method of dilution multiple (GB11903-1989). Conductivity of the wastewater was measured by a conductivity instrument (DDS-11A, Shanghai, China). The concentration of hydrogen peroxide was measured using a *p*-hydroxyphenylacetic acid (POHPAA) method. The Total Dissolved Solid (TDS) was determined by gravimetry. The value of TDS can be obtained according to eqn (1)

$$C = \frac{(W_1 - W_2) \times 1000 \times 1000}{V} \quad (1)$$

where C is the total dissolved solids of the wastewater (mg L^{-1}), W_1 is the total mass of evaporating dish and TDS (g), W_2 is the mass of free evaporating dish (g), V is the volume of the wastewater (mL).

3. Results and discussion

3.1 Characterization

3.1.1 Conductivity. The conductivity was detected by 4-point probes resistivity measurement system. As a result, the conductivity of B-nZVI was 15.9 10^{-3} S cm^{-1} which was better than that of Na-bentonite (0.3 10^{-3} S cm^{-1}) and activated carbon (12.5 10^{-3} S cm^{-1}).[22] So B-nZVI was more suitable to play the role of granulated electrode in 3D electrode system for treatment of wastewater.

3.1.2 XRD. The XRD patterns of Na-bentonite, fresh B-nZVI and recovered B-nZVI after reaction were shown in Fig. 2.

The XRD of B-nZVI contained a diffraction peak at $2\theta = 44.9°$ corresponding to the formation of Fe^0 (Fig. 2b).[23] The γ-Fe_2O_3

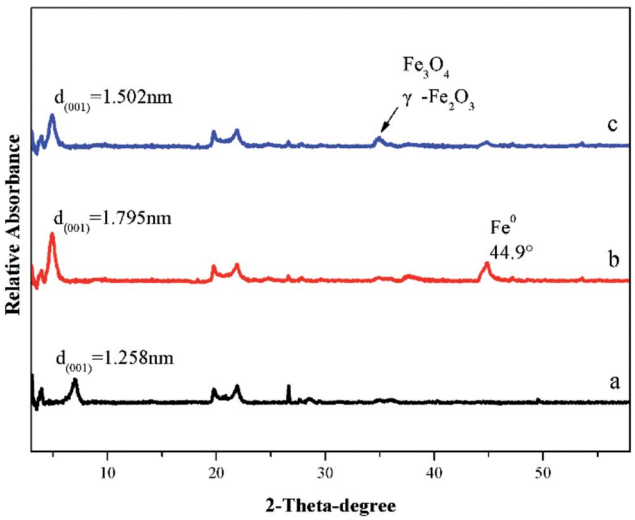

Fig. 2 XRD patterns. (a) Na-bentonite; (b) Fresh B-nZVI; (c) recovered B-nZVI.

Open Access Article. Published on 15 September 2017. Downloaded on 4/2/2026 6:58:39 AM.
This article is licensed under a Creative Commons Attribution 3.0 Unported Licence.

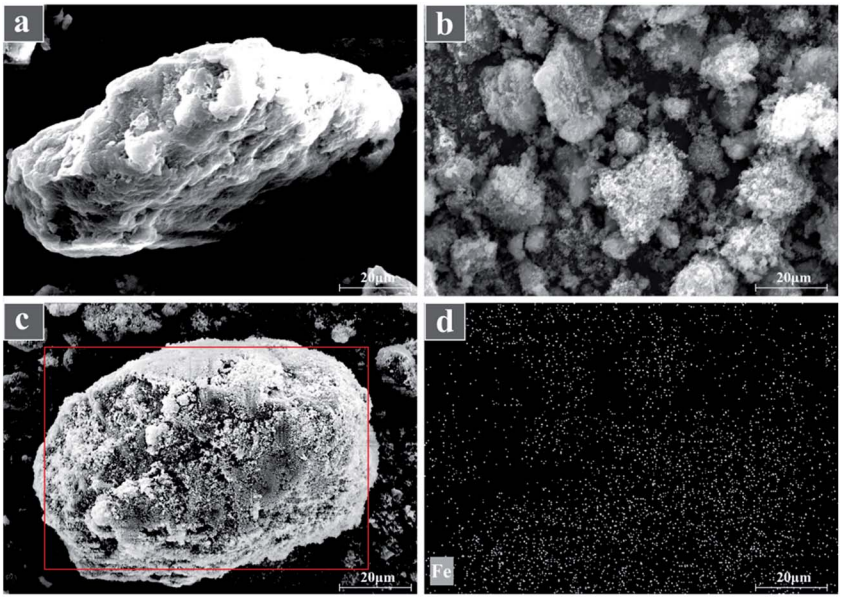

Fig. 3 SEM and EDS images: (a) bentonite; (b) nZVI; (c) B-nZVI; (d) disperation of iron on the surface of bentonite.

and Fe_3O_4 ($2\theta = 35.5^\circ$) can be detected in the sample after reaction (Fig. 2c), which was due to the transformation of Fe^0 to Fe^{2+}/Fe^{3+}.

The interlayer spacing of bentonite was calculated according to Bragg equation (eqn (2))

$$2d \sin \theta = n\lambda \quad (2)$$

where d is the value of interlayer spacing, θ is the diffraction angle of the characteristic peak, n is the diffraction order and its value is 1, λ is the diffraction wavelength of 0.15 nm.

The $d_{(001)}$ of Na-bentonite (Fig. 2a) was 1.258 nm and the $d_{(001)}$ of fresh B-nZVI (Fig. 2b) was 1.795 nm, which indicated that the layer spacing of the bentonite widened due to the insertion of Fe^0. However, after reaction, because of the transformation of Fe^0 in the sandwich of bentonite to Fe^{2+}/Fe^{3+}, the $d_{(001)}$ of recovered B-nZVI decreased (Fig. 2c). Therefore, it was concluded that Fe^0 particles were successfully generated and part of them inserted into the interlayer of the bentonite.

3.1.3 SEM and EDS. A dense surface is evident in Fig. 3a in which porous and lamellar structures possessing adsorption capacity were formed. In Fig. 3b, aggregation of nZVI was found, this was caused by van der Waal's forces and magnetic attraction between Fe^0 particles. The aggregation reduced the reactive activity of nZVI. This explained why nZVI are commonly fixed on support materials such as biochar, starch, and kaolinite for reducing the aggregation and increasing mechanical strength of nZVI.[24–26] Fig. 3c showed nZVI particles had evenly dispersed on the surface of bentonite and aggregation greatly weakened. The distribution of iron on bentonite surface was characterized by EDS (Fig. 3d), result found iron particles distributed uniformly on the bentonite surface. This further proved bentonite was able to disperse Fe^0 particles and could prevent the aggregation of nZVI effectively.

3.1.4 BET-N_2. The specific surface areas of bentonite, nZVI, fresh B-nZVI and recovered B-nZVI were obtained by a BET-N_2 surface area analyzer. The surface area of B-nZVI was 53 $m^2\ g^{-1}$, which was larger than that of nZVI (33.5 $m^2\ g^{-1}$). Therefore, the application of unsupported nZVI was limited in remediation activities.[27] The results further indicated that nZVI was effectively dispersed on the surface of bentonite, some nZVI was embedded into the interlayer of the bentonite successfully. The aggregation of nZVI was relieved prominently. After ten runs, the surface area of B-nZVI was reduced to 21.2 $m^2\ g^{-1}$ due to the consumption of nZVI.

3.1.5 PZC and CEC. The PZC of bentonite, nZVI, fresh B-nZVI and recovered B-nZVI was 3.5, 8.6, 7.3 and 5.2, respectively. As can be seen, the PZC of B-nZVI is larger than that of bentonite which was due to the evenly disperse of nZVI, this facilitated the anionic contaminants adsorbed on B-nZVI. After ten runs, the PZC of B-nZVI decreased compared with fresh B-nZVI, the main reason was the consumption of nZVI during the electrolysis process. Saturated adsorption of cationic contaminants on B-nZVI might be another reason.

The CEC of bentonite, fresh B-nZVI and recovered B-nZVI was 87.4 mmol/100 g, 62.5 mmol/100 g, 26.2 mmol/100 g, respectively. Results showed the CEC of B-nZVI was decreased compared with bentonite, this might due to the insertion of nZVI particles in layered structure of bentonite. However, the insertion of nZVI could also enhance the reducing ability and reactivity of B-nZVI. After ten runs, the CEC of B-nZVI was greatly decreased, this was because the saturated adsorption was achieved.

In conclusion, B-nZVI has both advantages of bentonite and nZVI.

3.2 Optimization of the operational parameters of 2D electrode system

A series of single factor experiments were undertaken to determine the optimum conditions for 2D electrode system, including current density, electrolysis time, and electrode plates distance.

 This journal is © The Royal Society of Chemistry 2017

Open Access Article. Published on 15 September 2017. Downloaded on 4/2/2026 6:58:39 AM.
This article is licensed under a Creative Commons Attribution 3.0 Unported Licence.

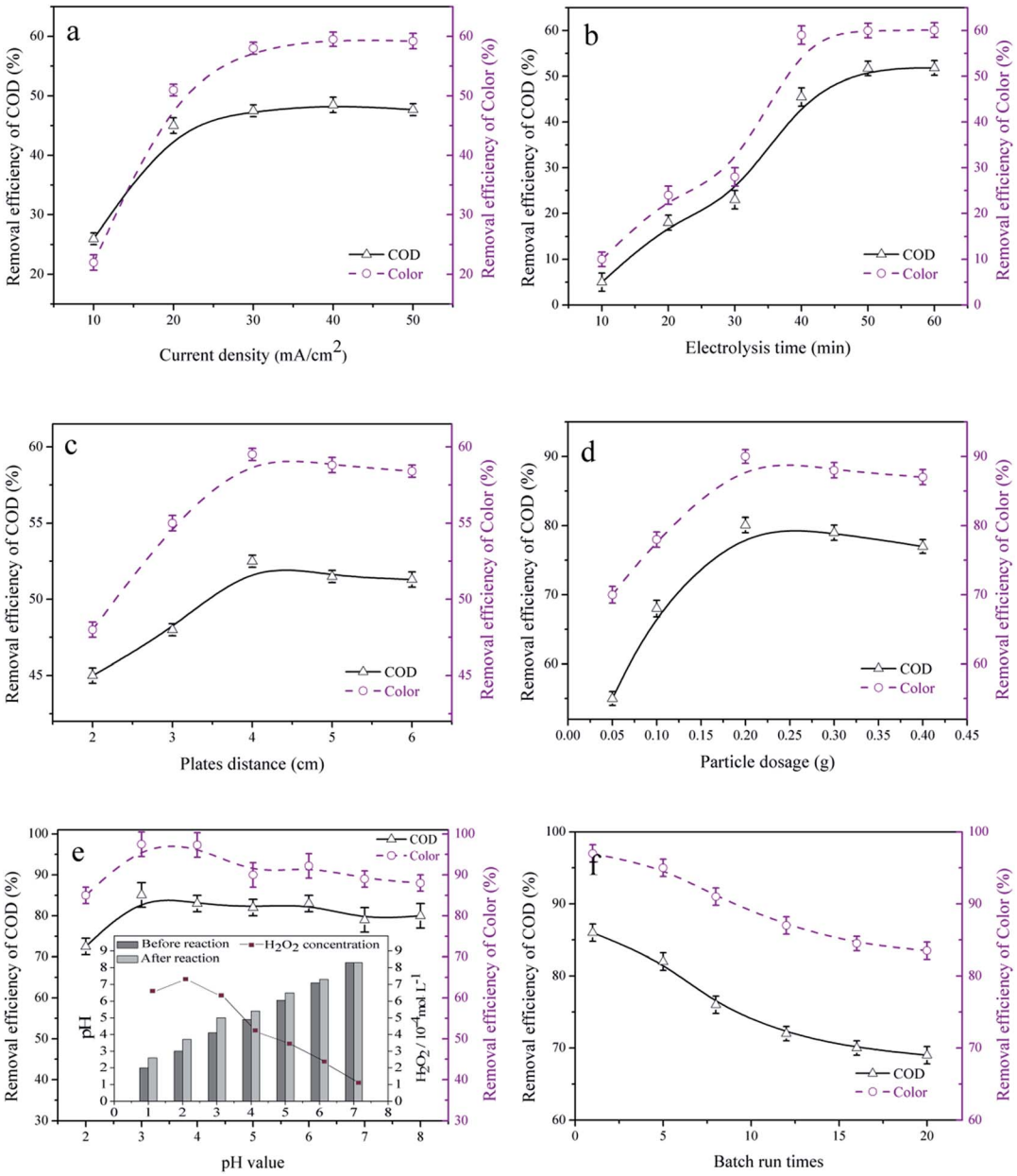

Fig. 4 Single factor experiments: (a) effect of current density; (b) effect of electrolysis time; (c) effect of electrode plates distance; (d) effect of dosage of B-nZVI; (e) effect of initial wastewater pH and its change before and after reaction; (f) effect of batch run times.

3.2.1 Effect of current density. The electrolysis was conducted with 4 cm electrode plates distance, stirring speed = 120 rpm, current density from 10 mA cm^{-2} to 50 mA cm^{-2}, initial pH = 8.0 (original wastewater), and electrolysis time = 50 min. The results were shown in Fig. 4a. The increase of current density lead to an increasing trend in COD removal rate and decolorization rate. This was due to the transfer rate of electrons increased substantially with the increase of current density, thereby enhanced the oxidation rate and reduction rate of pollutants. However, the removal efficiency of COD and color was not significant when the current density exceeded 40 mA cm^{-2}, this indicated excessive amounts of oxygen and hydrogen bubbles generated from the electrolysis of wastewater restrained contact of pollutants with the electrodes.[5] The optimal applied current density in the 2D system was 40 mA cm^{-2} to yield COD and color removal efficiencies of 48.5% and 59.5%, respectively, at an energy consumption of 10 kW h m^{-3} after 50 min.

3.2.2 Effect of electrolysis time. First, the electrolysis experiment was conducted at initial pH = 8.0, 40 mA cm^{-2}, 4 cm electrode plates distance, stirring speed = 120 rpm, and electrolysis time varied from 10 min to 60 min (Fig. 4b).

It was evident that a prolongation in electrolysis time led to an increase of COD removal and decolorization rate prior to 50 min. Yet, an extension of electrolysis time did not afford an obvious change. This trend was due to a decline in contact of

Open Access Article. Published on 15 September 2017. Downloaded on 4/2/2026 6:58:39 AM.
This article is licensed under a Creative Commons Attribution 3.0 Unported Licence.

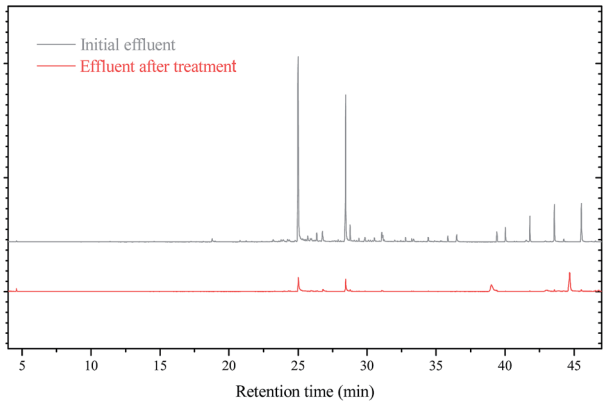

Fig. 5 The results of GC-MS of pulp and paper wastewater before and after reaction.

pollutants with the electrodes surface until 50 min at which point intractable by-products from incomplete oxidation of pollutants may level off the trend.

The optimum electrolysis time was 50 min where the COD and color removal efficiencies were 51.5% and 60.0%, respectively.

3.2.3 Effect of electrode plates distance. The current density of this electrolysis experiment was 40 mA cm^{-2} for 50 min with an electrode plates distance adjusted from 2 cm to 6 cm, initial pH = 8.0 (Fig. 4c), stirring speed = 120 rpm. A higher COD removal rate and decolorization rate was achieved from electrode plates distance of 4–6 cm. Nevertheless, when the distance was less than 4 cm, insoluble electrolytic product may contaminate the surfaces of electrode plates to block the flow and reduce effective contact sites. However, increase of the distance would increase the working voltage, the energy consumption would also be increased; thus, in consideration of these facts, the optimum distance of electrode plates was selected as 4 cm.

In conclusion, the optimum conditions of 2D electrode system were: current density = 40 mA cm^{-2}, electrolysis time = 50 min, and electrode plates distance = 4 cm with stirring speed = 120 rpm. Afterwards, B-nZVI granules were added into the 2D electrode system to afford a 3D system for further remediative activity.

3.3 Optimization of the operational parameters of 3D electrode system

3.3.1 Effect of dosage of B-nZVI. The main focus of this part is to investigate the effect of the dosage of B-nZVI on COD removal and decolorization rate of pulp and paper wastewater. Thus, different dosage (0.5 g L^{-1} to 4 g L^{-1}) of B-nZVI granular electrodes were added to 100 mL of wastewater (Fig. 4d).

When the dosage was less than 2 g L^{-1}, increases in COD removal and decolorization rate were very sharp; however, there was a slight decline when the dosage exceeded 2 g L^{-1}. Consequently, the maximum COD removal rate and decolorization rate were 80.1% and 90.0%, respectively. When the dosage was less than 2 g L^{-1}, the effective surface area of granulated electrodes increased with the increase of particle dosage. Furthermore, the transfer paths of electrons between plates were also be shortened, thus enhanced the efficiency of degradation. However, if the dosage of granulated electrodes increased to a certain extent (2 g L^{-1}), the number of suspended particles which was acted as working 3D electrodes would no longer increased. This could be attributed to two reasons: first, B-nZVI granules aggregated with increasing the dosage, hence total surface area decreased and diffusion path length of organic pollutants increased; second, the increase in B-nZVI dosage led to unsaturation adsorption sites, and many nano-scale zero-valent iron granules were oxidized to Fe_2O_3 and Fe_3O_4, thus resulted in the decrease of equilibrium adsorption capacity and reduction capacity of B-nZVI. The optimal dosage of B-nZVI was found to be 2 g L^{-1}.

3.3.2 Effect of initial pH of pulp and paper wastewater. pH was critical because it might affect the ionization state of B-nZVI and may trigger Fenton reactions in the 3D system in the presence of iron. Therefore, the initial pH of the target wastewater needed adjust during the process (Fig. 4e). When pH = 3.0, the highest removal efficiency of COD and color could reach 85.1% and 97.5%, respectively. During electrolysis, hydrogen peroxide would be generated through reduction of O_2 under acidic conditions and an indirect Fenton reaction would take place between added Fe^0 and H_2O_2 to generate hydroxyl radicals.[28–30] Meanwhile, Fe^{2+} was transformed to Fe^{3+} for the reaction with H_2O_2 and the oxidation at anode. In turn, Fe^{2+} could be regenerated by the reduction of Fe^{3+} at cathode and the reactions of Fe^{3+} with organic radicals and H_2O_2, such a cycle could provide sufficient Fe^{2+} for further Fenton reaction and effectively decreased the consumption of B-nZVI.[31]

When pH = 2.0, removal efficiency of COD and color was lower, the phenomenon can be attributed to that the saturated hydrogen ions providing a proton for H_2O_2 to form hydroxonium ions ($H_3O_2^+$, eqn (3)), which reduced the reactivity of H_2O_2.[32,33] Furthermore, $[Fe(H_2O)_6]^{2+}$ and $[Fe(H_2O)_6]^{3+}$ were the main species of Fe^{2+}/Fe^{3+} in solution at lower pH, which reacted slowly with H_2O_2.[34] Additionally, the scavenging effect of the $^{\bullet}OH$ by H^+ was severe (eqn (4)).[35–37] Thus, too low pH would weaken the degradation efficiency of pollutants. When pH increased from 4.0 to 8.0, the removal efficiencies of COD and color were decreased, not only by the decomposition of H_2O_2,[38,39] but also due to the formation of ferric hydroxide complexes.[40]

$$H_2O_2 + H^+ \rightarrow H_3O_2^+ \quad (3)$$

$$^{\bullet}OH + H^+ + e^- \rightarrow H_2O \quad (4)$$

pH of the wastewater varied with the change of the concentration of H^+. As shown in Fig. 4e, pH of every group increased after reaction, especially under the acidic conditions. The most obvious change of pH was at pH = 3.0. Fig. 4e also showed H_2O_2 concentration variation with B-nZVI dosage of 2 g L^{-1}. As can be seen, when pH = 3.0, the concentration of hydrogen peroxide reached its maximum, which was accumulated to 0.73 mmol L^{-1} at 50 min. The results indicated that the lower

 This journal is © The Royal Society of Chemistry 2017

Open Access Article. Published on 15 September 2017. Downloaded on 4/2/2026 6:58:39 AM.
This article is licensed under a Creative Commons Attribution 3.0 Unported Licence.

pH contributed to the generation of hydrogen peroxide. In other words, the main reason for the high removal efficiencies of COD and color at lower pH is the occurrence of Fenton reaction.

3.3.3 Effect of run times on the degradation of COD and color. The reusability of the B-nZVI granules was tested under calculated optimum conditions (Fig. 4f). The removal efficiency of COD and color decreased with increases in run times although they were high. This was likely because Fe^0 was oxidized to be Fe^{2+} and Fe^{3+} continuously, thus reducing the reducing ability of nZVI and the generation of hydrogen peroxide. However B-nZVI was stable enough to retain its activity.

3.4 Control experiments

Under the optimum conditions concluded above, the treatment experiments of pulp and paper wastewater using 2D system and B-nZVI alone without current were conducted. As a result, when current density = 40 mA cm^{-2}, electrolysis time = 50 min, electrode plates distance = 4 cm, pH = 3.0 with stirring speed = 120 rpm, the removal efficiencies of COD and color using 2D system were 50.1% and 61.2%, respectively. Without applying current, when pH = 3.0, B-nZVI dosage = 2 g L^{-1} with stirring = 120 rpm, the removal efficiencies of COD and color using B-nZVI alone were 21.5% and 26.2%, respectively.

As can be seen, the removal efficiency of COD and color using 3D system was better than the sum of the removal efficiency using 2D system and B-nZVI alone without current, the results indicated the existence of Fenton reaction, that is, hydroxyl radicals played an important role in 3D system.

3.5 Analysis of GC-MS

Fig. 5 showed the change of organic pollutants in initial and treated wastewater. The initial wastewater mainly contained toxic organic pollutants such as tetradecane, hexadecane, and octodecane as well as polycyclic aromatic hydrocarbons (PAHs, *e.g.*, naphthalene).[41] Following 3D electrode system tertiary treatment, most toxic and harmful substances decreased significantly. The results indicated that 3D system equipped with B-nZVI granules were much efficient to degrade pulp and paper wastewater.

3.6 Modelling of analytical results

Fig. 6 shows a possible degradation mechanism including electrolysis, adsorption and reduction of B-nZVI in pulp and paper wastewater. Because of decrease of initial pH, the Fenton-like reaction may be a critical reason for the degradation of organic compounds.

In 3D electrode system, when B-nZVI was added, its larger specific surface area and perfect conductivity, help to increase the rate of electron transfer sharply. The organic pollutants and its intermediates may be adsorbed by B-nZVI followed by combination of Fe^0 with the organic molecules and a reduction reaction happened. Unsaturated bonds in chromophores (colored) (principally from C=C, C=O and benzene) will be reduced by Fe^0 and thus decrease the color of the wastewater.

B-nZVI will be oxidized to Fe^{2+} by O_2 (eqn (5)).[42] The initial pH of the pulp and paper wastewater provides a chance for a Fenton-like reaction between B-nZVI and hydrogen peroxide

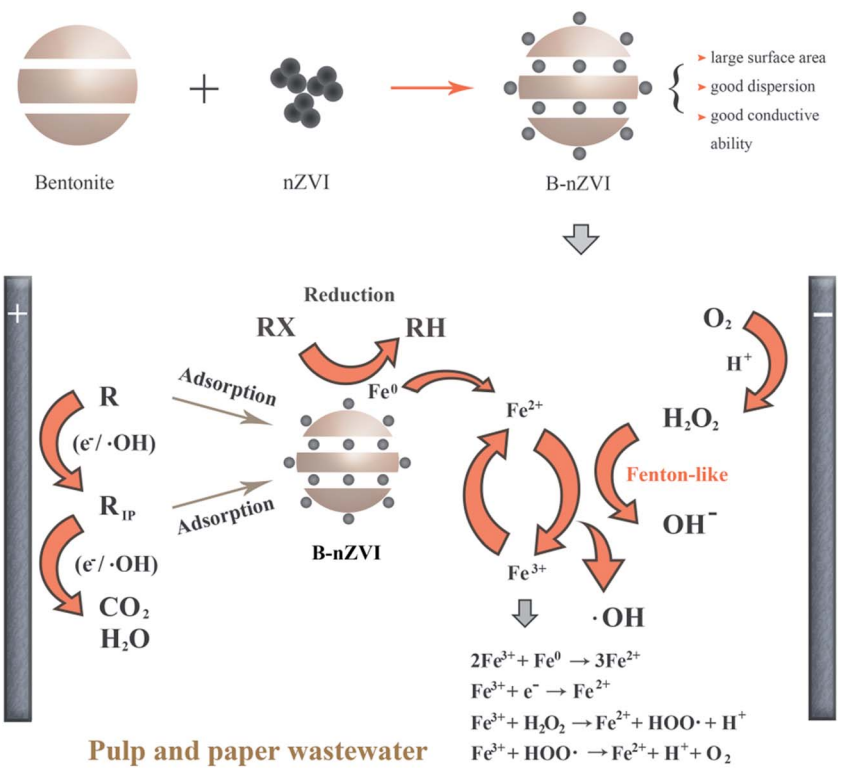

Fig. 6 Possible mechanism of degradation of organic pollutants in 3D electrode system.

Open Access Article. Published on 15 September 2017. Downloaded on 4/2/2026 6:58:39 AM. This article is licensed under a Creative Commons Attribution 3.0 Unported Licence.

(H_2O_2). O_2 will be reduced by H^+ and generate H_2O_2 (eqn (6)) on the cathode side. Therefore, plenty of $^{\cdot}OH$ with strong oxidizing power will be generated from the Fenton reaction between H_2O_2 and Fe^{2+} (eqn (7)).[43] Meanwhile, Fe^{3+} appears instantly being reduced to be Fe^{2+} to continue a cycle. Therefore, such a cycle can not only reduce the consumption of nZVI, but also oxidize organic substances efficiently.

$$2Fe^0 + O_2 + 2H_2O \rightarrow 2Fe^{2+} + 4OH^- \quad (5)$$

$$O_2 + 2H^+ + 2e^- \rightarrow H_2O_2 \quad (6)$$

$$Fe^{2+} + H_2O_2 \rightarrow {}^{\cdot}OH + OH^- + Fe^{3+} \quad (7)$$

4. Conclusions

The 3D electrode system consisting of a ruthenium/iridium coated titanium cathode and anode and B-nZVI granular electrodes is very effective for the remediation of pulp and paper wastewater. SEM and EDS suggests the layered structure of bentonite can reduce the aggregation of nZVI effectively. XRD illustrates that the bentonite may prevent nZVI from oxidation whereas BET-N_2 indicates B-nZVI has a much larger surface area than bare nZVI. The results of PZC and CEC suggest that B-nZVI has good adsorption performance and reactivity for the pollutants in wastewater. The COD value of the wastewater decreased from 296 mg L^{-1} to 59 mg L^{-1} while the decolorization rate reached 90.0% at conditions of current density = 40 mA cm^{-2}, electrolysis time = 50 min, electrode plates distance = 4 cm, and dosage of B-nZVI = 2 g L^{-1}. When the initial pH of wastewater was 3.0, because of the Fenton-like reaction, the maximum removal rate of COD was 85.1% (COD = 44 mg L^{-1}) and the decolorization rate of wastewater was 97.5%. The results of GC-MS proved that the 3D electrode system was efficient to remove organic substances in pulp and paper wastewater. Results proved B-nZVI filled 3D electrode system was an effective technology in the treatment of pulp and paper wastewater. It was found that the COD and color attained US EPA discharge standards (GB3544-2008) for the pulp and paper industry.

Conflicts of interest

There are no conflicts to declare.

Acknowledgements

The authors are grateful to be supported in part by the twelfth five-year National Key Technology R&D Program (2014BAC13B04).

References

1 M. Vepsäläinen, H. Kivisaari, M. Pulliainen, A. Oikari and M. Sillanpää, *Sep. Purif. Technol.*, 2011, **81**, 141.
2 D. Shao, W. Chu, X. Li, W. Yan and H. Xu, *RSC Adv.*, 2016, **6**, 4858.
3 C. H. Lee, E. S. Lee, Y. K. Lim, K. H. Park, H. D. Park and D. S. Lim, *RSC Adv.*, 2017, **7**, 6229.
4 J. Xing, D. Chen, W. Zhao, X. Peng, Z. Bai, W. Zhang, *et al.*, *RSC Adv.*, 2015, **5**, 53504.
5 C. Wang, Y. K. Huang, Q. Zhao and M. Ji, *Chem. Eng. J.*, 2014, **243**, 1.
6 C. Zhang, L. Zhou, J. Yang, X. Yu, Y. Jiang and M. Zhou, *Environ. Sci. Pollut. Res.*, 2014, **21**, 8398.
7 Y. Xiong, P. J. Strunk, H. Xia, X. Zhu and H. T. Karlsson, *Water Res.*, 2002, **35**, 4226.
8 L. Yan, H. Ma, B. Wang, Y. Wang and Y. Chen, *Desalination*, 2011, **276**, 397.
9 S. Y. Xue, B. S. Sun and Y. U. Bing, *Journal of Tianjin Institute of Textile Science and Technology*, 2005, **3**, 24.
10 X. W. He, L. Y. Liu, H. Wang, G. Zhang, J. W. Gong, H. Lin, *et al.*, *Water Sci. Technol.*, 2011, **63**, 2732.
11 G. Lv, D. Wu and R. Fu, *J. Hazard. Mater.*, 2008, **165**, 961.
12 W. Kong, B. Wang, H. Ma and L. Gu, *J. Hazard. Mater.*, 2006, **137**, 1532.
13 Y. P. Sun, X. Q. Li, J. Cao, W. X. Zhang and H. P. Wang, *Adv. Colloid Interface Sci.*, 2006, **120**, 47.
14 X. Q. Li, D. W. Elliott and W. X. Zhang, *Crit. Rev. Solid State Mater. Sci.*, 2006, **31**, 111.
15 B. Geng, Z. Jin, T. Li and X. Qi, *Sci. Total Environ.*, 2009, **407**, 4994.
16 J. Wang, G. Liu, T. Li and C. Zhou, *RSC Adv.*, 2015, **5**, 29859.
17 Y. Xu and D. Zhao, *Water Res.*, 2007, **41**, 2101.
18 K. G. Bhattacharyya and S. S. Gupta, *Adv. Colloid Interface Sci.*, 2008, **140**, 114.
19 H. Chu, Z. Wang and Y. Liu, *J. Environ. Chem. Eng.*, 2016, **4**, 1810.
20 Y. Lin, Z. Chen, Z. Chen, M. Megharaj and R. Naidu, *Appl. Clay Sci.*, 2014, **93**, 56.
21 Z. Xin, L. Shen, X. Q. Lu and Z. L. Chen, *Chem. Eng. J.*, 2010, **163**, 243.
22 A. Barroso-Bogeat, M. Alexandre-Franco, C. Fernández-González, J. Sánchez-González and V. Gómez-Serrano, *J. Phys. Chem. Solids*, 2015, **87**, 259.
23 Y. Y. Zhang, H. Jiang, Y. Zhang and J. F. Xie, *Chem. Eng. J.*, 2013, **229**, 412.
24 H. Dong, J. Deng, Y. Xie, C. Zhang, Z. Jiang, Y. Cheng, *et al.*, *J. Hazard. Mater.*, 2017, **332**, 79.
25 F. He and D. Y. Zhao, *Environ. Sci. Technol.*, 2005, **39**, 3314.
26 X. Zhang, S. Lin, Z. Chen, M. Megharaj and R. Naidu, *Water Res.*, 2011, **45**, 3481.
27 Ç. Üzüm, T. Shahwan, A. E. EroğLu, K. R. Hallam, T. B. Scott and I. Lieberwirth, *Appl. Clay Sci.*, 2009, **43**, 172.
28 X. H. L. Thi, M. Bechelany, J. Champavert and M. Cretin, *RSC Adv.*, 2015, **5**, 42536.
29 A. S. Giri and A. K. Golder, *RSC Adv.*, 2014, **4**, 6738.
30 B. Boye, M. M. Dieng and E. Brillas, *Environ. Sci. Technol.*, 2002, **36**, 3030.
31 Y. Lei, H. Liu, C. Jiang, Z. Shen and W. Wang, *J. Adv. Oxid. Technol.*, 2015, **18**, 47.

 This journal is © The Royal Society of Chemistry 2017

Open Access Article. Published on 15 September 2017. Downloaded on 4/2/2026 6:58:39 AM.
This article is licensed under a Creative Commons Attribution 3.0 Unported Licence.

32 B. G. Kwon, S. L. Dong, N. Kang and J. Yoon, *Water Res.*, 1999, **33**, 2110.
33 X. Han and D. K. Xia, *Sulphur Phosphorus Bulk Materials Handling Related Engineering*, 2004, **6**, 25, (in Chinese).
34 S. H. Bossmann, E. Oliveros, S. Göb, S. Siegwart, E. P. Dahlen, J. Leon Payawan, *et al.*, *J. Phys. Chem. A*, 1998, **102**, 5542.
35 J. Feng, A. X. J. Hu, P. L. Yue, H. Y. Zhu and G. Q. Lu, *Ind. Eng. Chem. Res.*, 2003, 2058.
36 M. Muruganandham and M. Swaminathan, *Dyes Pigm.*, 2004, **63**, 315.
37 H. Hassan and B. H. Hameed, *Chem. Eng. J.*, 2011, **171**, 912.
38 H. Shemer and K. G. Linden, *J. Hazard. Mater.*, 2006, **136**, 553.
39 Q. Wang and A. T. Lemley, *Environ. Sci. Technol.*, 2001, **35**, 4509.
40 C. L. Hsueh, Y. H. Huang, C. C. Wang and C. Y. Chen, *Chemosphere*, 2005, **58**, 1409.
41 N. N. Machalaba, N. N. Kuryleva, L. V. Okhlobystina, P. A. Matystsyn and I. A. Andriyuk, *Fibre Chem.*, 2000, **32**, 319.
42 A. Shimizu, M. Tokumura, K. Nakajima and Y. Kawase, *J. Hazard. Mater.*, 2012, **201**, 60.
43 E. Brillas, I. Sirés and M. A. Oturan, *Chem. Rev.*, 2009, **109**, 6570.